Materials Science-Poland, 30(4), 2012, pp. 348-354
http://www.materialsscience.pwr.wroc.pl/
DOI: 10.2478/s13536-012-0056-6

VERSITA

Preparation of crystal- controlled Y-TZP/Al_2O_3 nanocomposites

Y. FANG[1,2], Y. ZHANG[1], L. HU[1*]

[1] State Key Laboratory of Solid Lubrication, Lanzhou Institute of Chemical Physics, Chinese Academy of Sciences, Lanzhou, China

[2] Graduate School of Chinese Academy of Sciences, Beijing, China

ZrO_2–Y_2O_3–Al_2O_3 nanocrystalline powders with different grain sizes have been synthesized using a chemical coprecipitation method. Nano-powders were compacted uniaxially and densified in a vacuum hot-pressing furnace. Density, pore size distribution, grain size and composition of the composites were determined by various techniques, including BET gas absorption, field-emission scanning electron microscopy (FE-SEM) and X-ray diffraction (XRD). It has been shown that the porosity, grain and pore size of the ceramics can be controlled by the initial powder size and sintering temperature. Fully densified ceramics with narrow grain size distribution in the range of 100 $\sim$ 500 nm could be obtained.

Keywords: *ZrO_2–Y_2O_3–Al_2O_3; hot-pressing; crystal-controlled nanocomposites*

1. Introduction

High-performance ceramics with nanostructures ($<$ 100 nm grain size) are highly attractive materials due to their exceptional properties. During the past two decades, much effort has been directed toward preparing nanostructured ceramics. The manufacturing of nanoceramics implies a complete revision of the processing procedures concerning powder treatments, fabricating of green body and sintering in order to maintain the grain size characteristics of the initial powder. The main technological problems are related to the high specific surface area and surface activity of nano-sized powders, low packing density, and easy particle agglomeration during manufacturing. These features cause consequently differences in the grain growth during sintering [1, 2]. Several techniques for producing nanoceramics have been proposed by many researchers. New forming processes were used to improve the uniformity of green bodies and reduce the structural defects [3, 4]. Lots of sintering methods [5, 6] have been used to fabricate nanoceramics. In addition, nano-sized second phase particles dispersed within the matrix were used to inhibit its grain growth [7]. The microstructure of the material was constructed by dispersing nano-sized second phase particles within the matrix grains and at the grain boundaries. Thermal expansion mismatch between the matrix and second phase particles produces a marked improvement in mechanical properties such as fracture strength, fracture toughness, creep resistance, thermal shock resistance and wear resistance [8].

In the earlier studies, ZrO_2-Y_2O_3-Al_2O_3 nanocrystalline powders have already been prepared using a chemical coprecipitation method. On this basis, Y-TZP/Al_2O_3 nanoceramics were produced successfully by the authors [9], using pressureless sintering at 1200 °C. The presence of Al_2O_3 inhibits the grain growth and enhances the mechanical properties of pure Y-TZP ceramics. But during the pressureless sintering, the sample size has a great impact on the sintering process. Consequently, the fabrication of large-sized dense nanocrystalline ceramics is very difficult since an inevitable grain growth occurs at relatively high sintering temperatures which are needed for densification. Therefore, hot-pressing appears as a very appropriate technique to densify nanocrystalline ceramics. It is expected to decrease

*E-mail: zhysh@licp.cas.cn

the densification temperature and result in a finer grain size [10].

Actually, for structural material, researchers care about both grain size and their performance. It is very important to confirm the range of grain size within which the material shows the best performance. Therefore, one of the primary questions is how to prepare the nanocomposites with controllable grain size. The present work intends to examine the various powder properties and their effects on the compact behavior, densification mechanisms, hot-pressing parameters and microstructure of the bulk ceramics.

2. Experimental procedure

Homogeneous, 5 mol % Al_2O_3 doped ZrO_2(3Y) nano-sized powders with different grain sizes were synthesized by coprecipitation method. X-ray diffractometer (XRD, D/max-RB) was used to reveal the crystalline phases and grain size of the calcined powders. The mean grain size of powders was estimated from the full width at half maximum (FWHM) by the Scherrer equation and confirmed by transmission electron microscope (TEM, JEM1200EX). The green compact pellets were obtained by uniaxial pressing at 300 MPa for 5 min in air at room temperature. Geometric method was used to measure the green compact pellets density. BJH pore diameter distributions of the green compact were obtained from N_2 adsorption-desorption isotherms (ASAP-2010) at 77 K.

The equipment used for hot-pressing was a vacuum hot-pressing furnace (ZT-63-20Y, China). It permits densifying under a load of up to 20000 kg at temperatures up to 2000 °C. The dies made of graphite with internal diameters of 24 mm were used to prepare the samples. The apparatus was equipped with a digital comparator with ±1 μm accuracy, which allows dilatometric measurements. The procedure is to apply first a constant pressure (here in general P = 30 MPa) and then to increase temperature with a programmed rate of 10 °C/min. After reaching the desired temperature, the sample was held at this plateau for 1 h and directly cooled. Archimedes principle was used to measure the bulk density. XRD (D/max-RB) was used to reveal the crystalline phases of sintered samples. The microstructures of the ceramics were observed using field-emission scanning electron microscopy (FE-SEM, JEOL JSM-6701F).

Table 1. Temperature of calcinations and initial powder particle size d_i, green density ρ_i and pore size of the green body (P = 0.3 GPa, T = 25 °C).

$T_{calcination}$ (°C)	ρ_i (%)	Pore size (nm)	d_i (nm)	
			Scherrer	TEM
700	39 ± 2	4.6	8 ± 2	10 ± 3
1000	44 ± 3	4.9	11 ± 3	12 ± 4
1200	58 ± 5	6.2	35 ± 4	38 ± 6
1300	63 ± 4	8.2	72 ± 6	75 ± 8

3. Results and discussion

3.1. Morphological properties and compaction behavior of powders

Fig. 1 shows a set of the typical TEM micrographs of the ZrO_2(3Y)/Al_2O_3 powders calcined at different temperatures. It can be easily found that about 10 nm ZrO_2(3Y)/Al_2O_3 powders were obtained at 700 °C, 12 nm at 1000 °C, 38 nm at 1200 °C and 75 nm at 1300 °C. Fig. 2 compares the green densities achieved with the final compaction pressure for ZrO_2(3Y)/Al_2O_3 powders calcined at 700 °C. As can be seen in Fig. 2, the relative density is a linear function of the compaction pressure. The linear slope indicates that the powders are either nonagglomerated or with very low agglomerate strength (< 40 MPa) [7]. Also, the results show that relatively high applied pressure is required to achieve high green densities. The average grain sizes and standard deviations, determined by the Scherrer equation and TEM observations, are summarized in Table 1 for powders calcined at 700, 1000, 1200 and 1300 °C for 2 h. The green densities obtained by cold compaction at 300 MPa (Table 1) show particle size dependence. During cold compaction, densification occurs by partial deagglomeration or by rearrangement due to sliding, which depends on granulometric characteristics of the initial powder. The increased green density may be due to better packing associated with small parti-

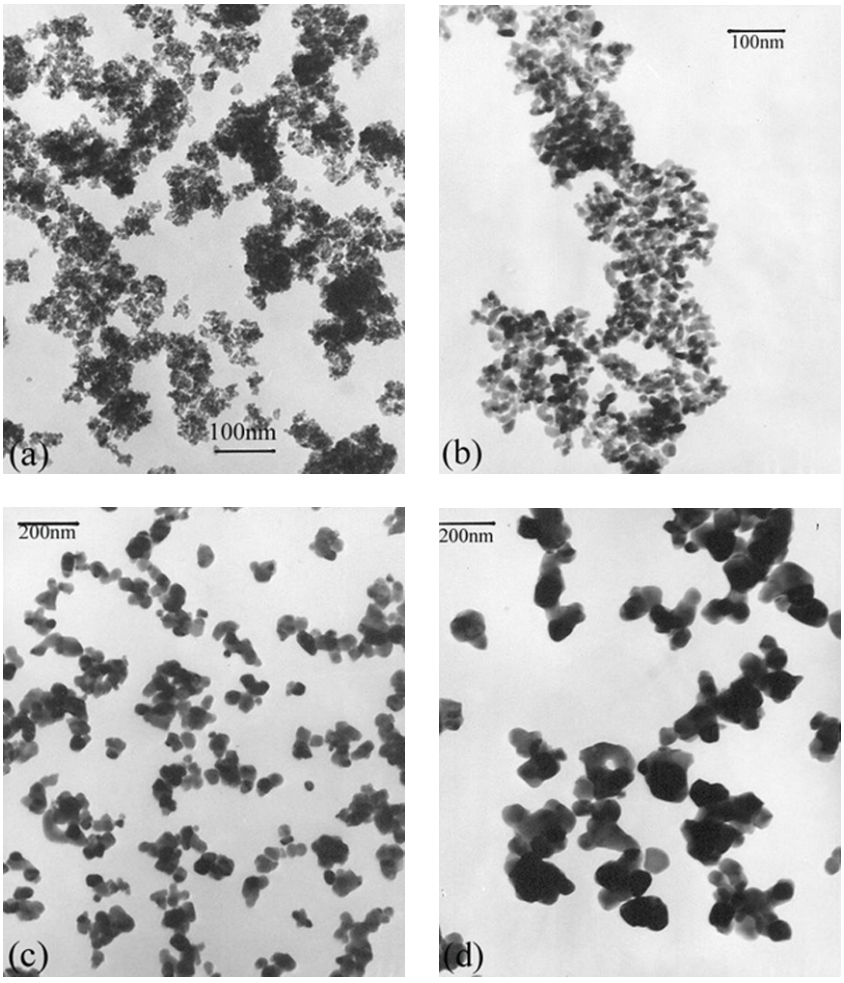

Fig. 1. TEM micrographs of the nano $ZrO_2(3Y)/Al_2O_3$ powders calcined at different calcinations temperatures: (a) 700 °C; (b) 1000 °C; (c) 1200 °C and (d) 1300 °C.

cles, filling the voids between the bigger ones. This is why the green density increases with the relative width of the particle size distribution, which increases here with the particle size [5].

Table 1 also shows the gradual increase in the pore diameter of the green body with the increasing powder size. A representation of nitrogen adsorption isotherms and the pore size distribution for the green bodies fabricated from the 10 nm and the 75 nm powders are shown in Fig. 3 and 4. All the adsorption isotherms belong to type IV of the IUPAC classification, indicating that the samples are mesoporous. The green body fabricated by 75 nm powder exhibits two peak distributions, one sharp peak at 2–6 nm, the other weak shoulder peak at

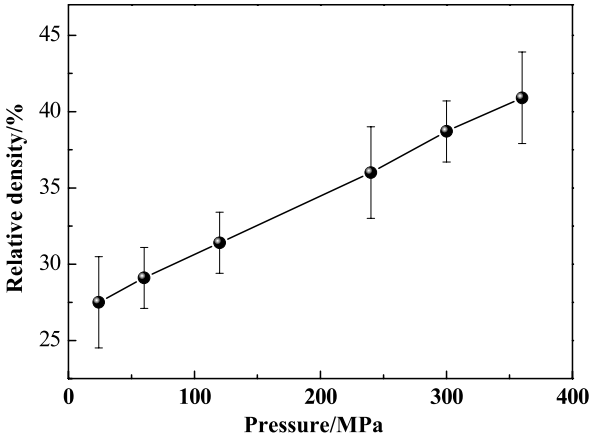

Fig. 2. Compaction behavior of $ZrO_2(3Y)/Al_2O_3$ powders calcined at 700 °C.

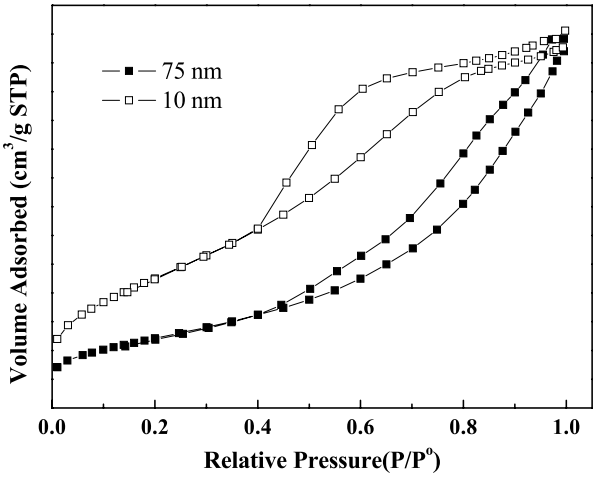

Fig. 3. Nitrogen adsorption isotherms of green bodies fabricated from the 10 nm and the 75 nm powders.

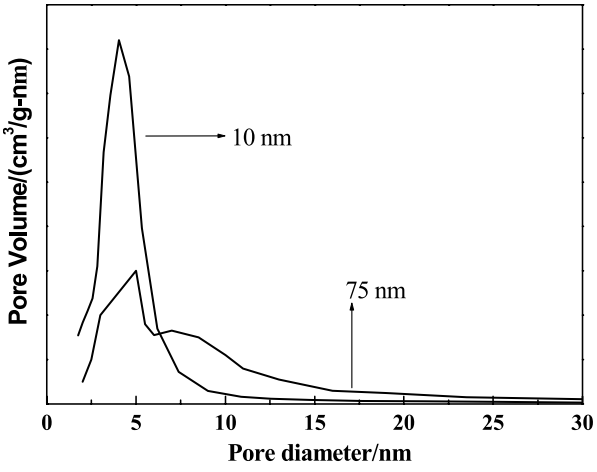

Fig. 4. Pore size distribution of green bodies fabricated from the 10 nm and the 75 nm powders obtained using the BJH model.

6–20 nm, and the average pore size of 8.2 nm. That of the green body based on 10 nm powder exhibits a narrow distribution (2–8 nm) with a single-peak located at a pore radius of 4.6 nm. It can be seen that the powder size has a great influence on the pore distribution and average pore size of the green body. Small size of powder particle may reduce the pores produced by the secondary particles, decrease the agglomeration of particles, and make pore size smaller and its distribution narrower.

Table 2. Initial powder particle size d_i, relative density ρ of material sintered at 1400 °C, densification temperature T_f and final grain size d_f of the nanocomposites.

Sample	d_i (nm)	ρ (%)	T_f (°C)	d_f (nm)
A	10 ± 3	98 ± 2	1400 °C	100 ± 50
B	12 ± 4	97 ± 2	1400 °C	150 ± 80
C	38 ± 6	91 ± 2	1450 °C	250 ± 120
D	75 ± 8	86 ± 2	1500 °C	300 ± 150
E	75 ± 8	86 ± 2	1600 °C	500 ± 150

3.2. Densification and microstructure

The initial powder particle size, relative density of material sintered at 1400 °C, the grain size of sintered materials when its density approaches the theoretical value and the densification temperature are summarized in Table 2. From Table 2, it can be found that the samples A and B achieved similar densities after sintering at 1400 °C, but only a relative density of 91 % and 86 % for the samples C and D was obtained at the same temperature. The densification temperature was increased by 100 °C while the initial powder size increased from 10 nm to 75 nm. Fig. 5(a–e) show SEM micrographs of the five fully densified ceramics fabricated from powders of different initial particle sizes. Five ceramics show a dense microstructure and the microstructures of the as-sintered nanocomposites are typical of ceramics in the final stage of sintering. At the same time, some uniaxial grains and polyhedral morphology can be also found in the SEM micrographs, with average grain sizes of 100 nm (Fig. 5a), 150 nm (Fig. 5b), 250 nm (Fig. 5c), 300 nm (Fig. 5d) and 500 nm (Fig. 5e), indicating that strong grain growth occurred during the sintering. In addition, the EDS analysis exhibited clear peaks of Zr, O and Al from any detected site. XRD analysis showed that the nanocomposites are mainly composed of tetragonal zirconia and a few a-Al_2O_3. As the grain size of nanocomposites grows to 500 nm, a small amount of the monoclinic zirconia phase forms. The photograph of sintered Y-TZP/Al_2O_3 specimen is given in Fig. 6. It is clear that large-size dense Y-TZP/Al_2O_3 nanocomposites with controlled grain size ($100 \sim 500$ nm) can be obtained by hot-pressing.

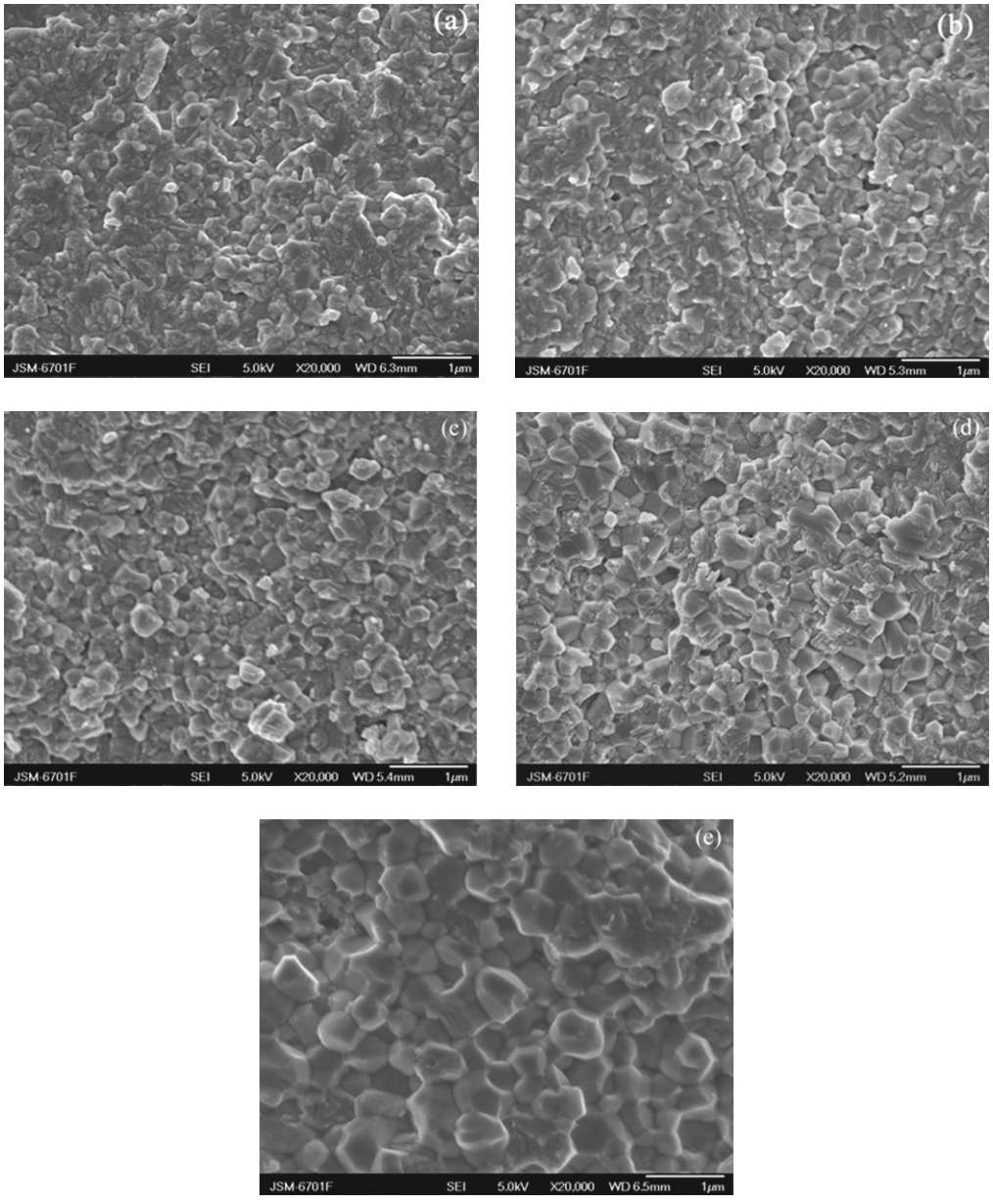

Fig. 5. SEM photographs of Y-TZP/Al_2O_3 nanocomposites with average grain sizes of 100 nm (a), 150 nm (b), 250 nm (c), 300 nm (d) and 500 nm (e).

3.3. Discussion

The results presented above show that the initial powder size has an important influence on the densification temperature. The increased powder size induces an increase in the densification temperature. As a consequence, an evident grain growth occurs at relatively high sintering temperatures. In general, the driving force for densification in hot-pressing arises from the applied stress and particle surface tension [11]:

$$DF = \gamma\Omega K + gP_a \tag{1}$$

where DF is the driving force for densification, γ is surface energy, Ω is the molecular volume, K is a constant related to the pore size, g is a geometric constant, P_a is the external applied pressure. It can be seen from Equation (1) that when the pressure is

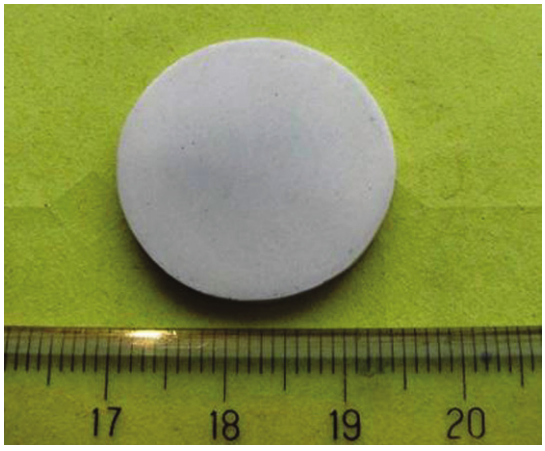

Fig. 6. Sintered specimen body in the present study.

kept constant, particle surface tension has a very important effect on the driving force for densification. Smaller particles have a higher sintering activity because of their larger surface energy, which results in higher driving force for sintering at lower temperature. In addition, it is generally accepted that the densification of ceramics or the shrinkage of pores during sintering occurs by diffusion, and that the driving force for such diffusion is the reduction of the internal surface area associated with pores [1, 12]. The instantaneous driving force for diffusion is assumed to be inversely proportional to the pore's radius of curvature. The driving force for sintering is often written as [1]:

$$\sigma = A\gamma/r \tag{2}$$

where A is a geometric constant with a value of 1 (cylindrical pore) or 2 (spherical pore), γ is the surface tension associated with the pore/solid interface, and r is the pore radius (inverse of pore curvature). Using Equation (2), the driving force for sintering is 244 MPa assuming $\gamma = 1$ J·m^{-2} for the pores of 8.2 nm. In comparison, the ceramics with pores of about 4.6 nm has a sintering force of 435 MPa, the σ value increased by 78 % accordingly when other factors are kept unchanged.

Nieh and Wadsworth [13] reported superplasticity in bulk specimens of Y-TZP (300-nm grain size) at temperatures below 1500 K and strain rates of the order of 10^{-4}s^{-1}.They predicted that superplasticity would further accelerate densification of the nanocrystalline material under external load, particularly at the early stage of the process [13, 14]. The grain-size effect on superplasticity has been often discussed in the literature and can be explained by the fact that grain boundary sliding is the dominant deformation mode. High-temperature deformation behavior in fine-grained ceramics is usually described by [15]:

$$\dot{\varepsilon} = B\frac{\sigma^n}{d^p}\exp\left(-\frac{Q}{RT}\right) \tag{3}$$

where B is a numerical constant, σ is the flow stress with exponent n, d is the grain size with exponent p, Q is the apparent activation energy, R is the gas constant and T is the temperature. From Equation (3), it can be concluded that the grain size reduction results in a decrease in the superplastic deformation temperature.

Based on the above discussion, it can be concluded that the smaller initial powder size and average pore size of the compacts, the narrower pore distribution and the lower superplastic deformation temperature make nanoceramics easier to densification at low temperature.

4. Conclusions

High quality homogeneous Al_2O_3 doped yttria-zirconia nano-powders can be obtained using a co-precipitation method. By controlling the calcination temperature properly, ZrO_2-Y_2O_3-Al_2O_3 powders with narrow grain size distribution in the range of 6–83 nm can be obtained. The pore distribution and average pore size of compacts show particle size dependence; the pore size becomes smaller and its distribution narrower with decreasing particle size.

The presented work also shows that dense Y-TZP/Al_2O_3 nanocomposites with controlled grain size (100 $\sim$ 500 nm) can be obtained by hot-pressing using the powders with different grain sizes. The sintered bodies were composed mainly of tetragonal and small amount of a-Al_2O_3 phase. The obvious advantage of the green compact fabricated from the powder with a smaller size is the fact that the sintering temperature decreased to the value as low as 1400 °C, and hot-pressing to sinter at low temperature allowed us to keep a small grain size.

Ceramics based on 10 nm powder were sintered at 1400 °C with a mean grain size of 100 nm. The reason of the good sintering behavior is believed to be the decrease in the pore size, final grain size and superplastic deformation temperature.

Acknowledgements

This study was supported by National Natural Science Foundation of China (Grant No. 50902132, 51175493), the Program of the Light of the Chinese Academy of Sciences in Chinas Western Region (2010), and the China National Science and Technology Program of 973 (2011CB706603).

References

[1] MAYO M.J., *Int. Mater. Rev.*, 41 (1996), 85.
[2] BELLOS A., SCITI D., GUICCIARDI S., *J. Eur. Ceram. Soc.*, 24 (2004), 3295.
[3] ZHANG Y.S., HU L.T., CHEN J.M., LIU W.M., *Adv. Eng. Mater.*, 8 (2006), 271.
[4] MILLER K.T., ZUKOSKI C.F., *J. Am. Ceram. Soc.*, 77 (1994), 2473.
[5] WEIBEL A., BOUCHET R., DENOYEL R., KNAUTH P., *J. Eur. Ceram. Soc.*, 27 (2007), 2641.
[6] CHAIM R., *Mat. Sci. Eng. A-Struct.*, 443 (2007), 25.
[7] SRDIC V.V., WINTERER M., HAHN H., *J. Am. Ceram. Soc.*, 83 (2000), 1853.
[8] CHOI S.M., AWAJI H., *Sci. Technol. Adv. Mat.*, 6 (2005), 2.
[9] ZHANG Y.S., CHEN J.M., HU L.T. , LIU W.M., *Mater. Lett.*, 60 (2006), 2302.
[10] WEIBEL A., BOUCHET R., BOUVIER P., KNAUTH P., *Acta Mater.*, 54 (2006), 3575.
[11] SKANDAN G., HAHN H., KEAR B.H., RODDY M., CANNON W.R., *Mater Lett.*, 20 (1994), 305.
[12] GAO L., LI W., WANG H.Z., ZHOU J.X., *J. Eur. Ceram. Soc.*, 21 (2001), 135.
[13] NIEH T.G., WADSWORTH J., *Acta. Metall. Mater.*, 38 (1990), 1121.
[14] BOURELL D.L., PARIMAL, KAYSSER W.A., *J. Am. Ceram. Soc.*, 76 (1993), 705.
[15] NICHOLS F.A., *Acta Metall.*, 28 (1980), 663.

Received 2012-01-13
Accepted 2012-10-26